PERGAMON

International Journal of Heat and Mass Transfer 46 (2003) 1395–1407

International Journal of HEAT and MASS TRANSFER

www.elsevier.com/locate/ijhmt

# Interactions between molten metal droplets impinging on a solid surface

R. Ghafouri-Azar, S. Shakeri, S. Chandra, J. Mostaghimi *

*Centre for Advanced Coating Technologies, Department of Mechanical and Industrial Engineering, University of Toronto, 5 King's College Road, Toronto, Ontario M5S 3G8, Canada*

Received 7 May 2002; received in revised form 17 September 2002

**Abstract**

We photographed molten tin droplets (2.2 mm diameter) landing off-center on a circular splat formed by the impact and solidification of another, identical drop. Final splat shapes were sensitive to the spacing between droplet centers, which was varied from 1.0 to 5.0 mm. We used a three-dimensional model of spreading and solidification to simulate interactions between droplets. The model applied a fixed-grid Eulerian control volume method to solve the fluid dynamics and energy conservation equations. A volume-of-fluid algorithm was used to track free surface deformation. Predictions of droplet shapes during impact from the model agreed well with photographs. By following *temperature variations* at different points on the surface of the first splat we could identify locations where remelting occurred and the splats fused together. Splat shapes observed in experiments with large tin droplets qualitatively resembled those obtained by plasma-spraying nickel powders on a steel surface.


*Keywords:* Spray forming; Spray coating; Droplet impact; Free surface flow; Solidification

## 1. Introduction

Several numerical models [1–9] have been developed in recent years to simulate impact and freezing of molten metal droplets on a solid substrate. These models are intended for use in applications such as spray coating or spray forming, in which molten droplets accelerated by a gas jet land with high velocity on a solid surface. Splats formed by flattened droplets fuse together as they solidify, forming a dense layer. The properties of coatings or objects produced by this method depend on the shapes and temperature history of individual splats, which can be predicted using numerical codes.

Since the dynamics of single droplet impact have been thoroughly investigated, and are reasonably well understood, the obvious next step is to model the formation of solid layers by the deposition of many droplets. However, this problem has proved so complex that few researchers have attempted it. Simulating impact of droplets on an uneven surface requires a fully three-dimensional model, which places severe demands on computing resources. Modeling the impact and solidification of just a single drop requires many hours of computer time [9]; simulating the build-up of even a small area of coating, which may consist of several thousand droplets, is clearly impractical.

Avoiding this brute-force approach to simulating spray coating formation, we have attempted a less computationally intensive technique. Our model includes a set of rules that specify the final splat shape as a function of droplet impact conditions [10]. Given the velocity, size and thermophysical properties of a droplet, and the topology of the substrate it lands on, the model

* Corresponding author. Tel.: +1-416-978-5604, fax: +1-416-946-8252.

*E-mail address:* mostag@mie.utoronto.ca (J. Mostaghimi).

0017-9310/03/$ - see front matter 
PII: S0017-9310(02)00403-9

**Nomenclature**

| | |
|---|---|
| $A$ | splat area |
| $C$ | specific heat |
| $D$ | droplet diameter |
| $D_h$ | splat equivalent diameter ($= 4A/P$) |
| $d$ | diameter of droplet |
| $f$ | volume of fluid fraction |
| $\vec{F}_b$ | body force |
| $h$ | enthalpy |
| $H_f$ | latent heat of fusion |
| $k$ | thermal conductivity |
| $L$ | offset distance |
| $\hat{n}_l$ | liquid free surface unit normal |
| $\hat{n}_s$ | solidification front unit normal |
| $P$ | splat perimeter |
| $p$ | pressure |
| $q$ | heat flux |
| $R_c$ | thermal contact resistance |
| $t$ | time |
| $T$ | temperature |
| $T_m$ | melting temperature |
| $v$ | volume |
| $\vec{V}$ | velocity |

*Greek symbols*

| | |
|---|---|
| $\alpha$ | thermal diffusivity |
| $\beta$ | energy equation enthalpy coefficient |
| $\gamma$ | angle between $\hat{n}_l$ and $\hat{n}_s$ |
| $\Theta$ | liquid–solid volume fraction |
| $\theta_{ls}$ | liquid–solid contact angle |
| $\nu$ | kinematic viscosity |
| $\xi$ | spread factor |
| $\rho$ | density |
| $\phi$ | energy equation source term |

assigns a shape to the solidified splat. Accounting for substrate shape proved to be the most difficult task in developing spreading rules. We assumed that droplet spreading was influenced solely by the nearest previously deposited splat under it. Only two-droplet interactions were considered while more complex effects were neglected. We used a three-dimensional numerical model of droplet impact to predict what the final shape would be when a droplet landed on a previously deposited splat, with varying offset distances between the centers of the two drops. This—admittedly simple—method gave predictions for coating structure that appeared quite reasonable when compared with experimental data.

This paper describes a joint experimental and numerical study undertaken to test the abilities of our model to accurately predict shapes of splats formed by two-droplet interactions. Previous models [11,12] of sequential droplet deposition assumed that their centers were coincident, that the surface of the bottom splat was perfectly flat, and that heat transfer was much slower than the spreading rate of the droplets. None of these assumptions may be valid in applications of practical interest. Solidification of a molten droplet can have a strong effect on its spreading and final shape, and in a spray process droplets will land at random locations on an uneven surface.

We photographed the impact of molten tin droplets (2.2 mm diameter, 2.5 m/s impact velocity) on splats formed by the spreading and solidification of other, identical droplets. The distance between the centers of the two drops ($L$) was varied from 1 to 5 mm. We used a three dimensional numerical code to simulate droplet impact and compared predicted splat shapes with photographs. The results gave us insight into the dynamics of droplet interactions, and allowed us to gauge the accuracy of predictions from the model.

## 2. Experimental method

The experimental apparatus was a modified version of the one used earlier by Aziz and Chandra [13], who have described it in detail. A schematic diagram of it is shown in Fig. 1. Single tin droplets were released from the tip of a stainless steel needle (1.588 mm OD and 0.254 mm ID) inserted into the bottom of a heated chamber filled with molten tin. The diameter of the needle was so small that surface tension prevented the tin from flowing out. Rapidly opening and closing a solenoid valve for 10 ms sent a nitrogen gas pulse from a 69 kPa supply to the molten metal chamber, forcing out a droplet on demand. The gas in the droplet generator then escaped to the atmosphere though a vent, relieving the pressure inside it and preventing further droplets from escaping. By adjusting the opening of the needle valve through which the gas was vented the size of droplets produced could be varied. All tests described in this paper were done with 2.2 mm diameter tin droplets.

Droplet fell under their own weight onto a stainless steel test surface, traveling through a 25.4 mm diameter aluminum tube that was heated using a rope heater and landing with a velocity of 2.5 m/s on the test surface. Calculation of heat loss from droplets during their fall [14] showed that their temperature at the moment of impact was approximately 240 °C. The experiment was performed in a nitrogen atmosphere to prevent tin droplets from oxidizing. The test surface was placed

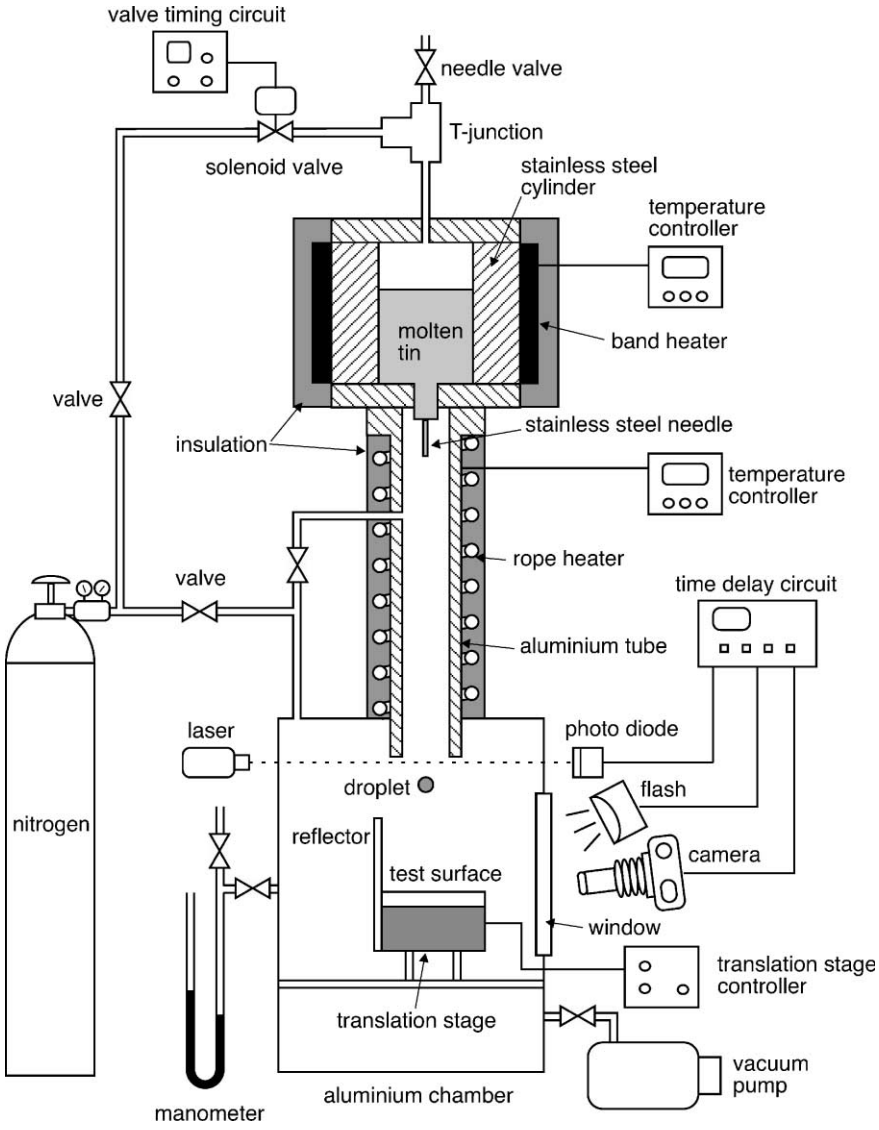


Fig. 1. Schematic diagram of experimental apparatus.

inside an aluminum chamber (0.3 m × 0.3 m × 0.15 m in size) that was first evacuated with a vacuum pump and then filled with nitrogen. A water manometer was used to measure the pressure inside the chamber and ensure that it remained constant.

Droplets landed on a 50.8 mm square and 6.4 mm thick stainless steel plate. The test surface was mounted on a small optical stage whose movement was controlled with a programmable controller. After the first droplet was released it was allowed to cool down and solidify. The test surface was then moved through the required distance (1–5 mm) and the second droplet deposited on top of the first.

Droplet impact was photographed using a single shot flash photographic method [13]. Droplets were photographed at a single instant during impact by activating a 8 μs duration flash. As a droplet fell it passed through a laser beam, whose interruption was used to trigger the flash. By varying the interval between droplet release and the flash, different stages of impact were recorded using a Nikon E3 digital camera, and the entire process of droplet deformation pieced together from these pictures.

## 3. Numerical method

### 3.1. Fluid dynamics and heat transfer of spreading

Fluid dynamics in the deforming droplet is governed by mass and momentum conservation equations:

$$\nabla \cdot \vec{V} = 0, \tag{1}$$

$$\frac{\partial \vec{V}}{\partial t} + \nabla \cdot (\vec{V}\vec{V}) = -\frac{1}{\rho}\nabla p + v\nabla^2 \vec{V} + \frac{1}{\rho}\vec{F}_b, \tag{2}$$

where $\vec{V}$ is the velocity vector, $p$ the pressure, $\rho$ the density, $v$ kinematic viscosity and $\vec{F}_b$ body forces acting on the fluid. The fluid flow was assumed to be Newtonian, laminar and incompressible. It was assumed that only normal stresses were exerted on the free surface of droplets and any effect of ambient air on their motion was neglected. The governing equations were discretized using finite volume techniques on a 3-D Eulerian structured grid. The volume-of-fluid (VOF) algorithm was

Table 1
Properties of tin and stainless steel (AISI 304) used in the numerical analysis

| Property | Tin | Stainless steel (AISI 304) | | |
|---|---|---|---|---|
| | (25–240 °C) | 27 °C | 127 °C | 327 °C |
| Density ($\rho$, kg/m$^3$) | 6970 | 7900 | 7900 | 7900 |
| Specific heat ($C$, J/kg K) | 244 | 477 | 515 | 557 |
| Thermal conductivity ($k$, W/m K) | 33.6 (fluid)<br>62.2 (solid) | 14.9 | 16.6 | 19.8 |
| Kinematic viscosity ($v$, m$^2$/s) | $2.75 \times 10^{-7}$ | – | – | – |
| Surface tension (N/m) | 0.526 | – | – | – |

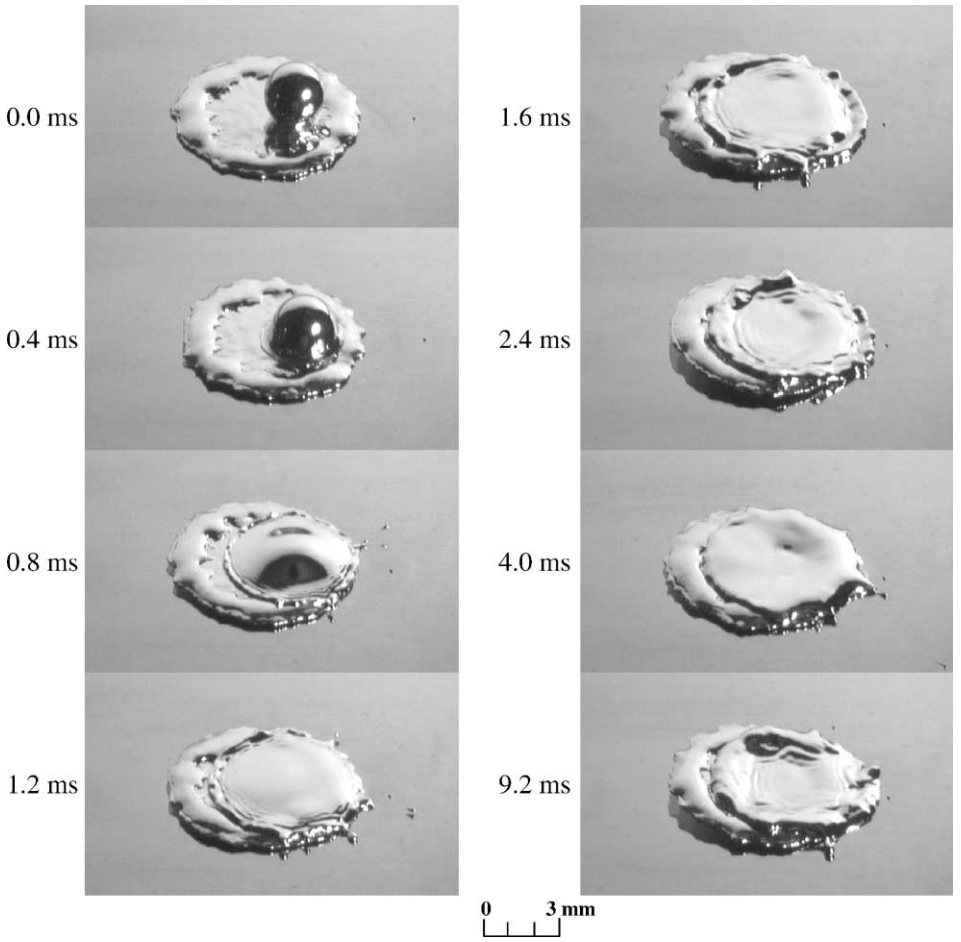


Fig. 2. Impact of a 2.2 mm diameter tin droplet landing with a velocity of 2.5 m/s on a splat formed by depositing another identical drop. The center of the second droplet is offset 1.0 mm from that of the first.

used to track the free surface deformation. The volume-of-fluid ($f$) is defined as the fraction of a cell volume occupied by fluid ($f = 1$ for a fully occupied cell by the fluid, $f = 0$ for an empty cell and $0 < f < 1$ for an interface cell). The advection equation of $f$,

$$\frac{\partial f}{\partial t} + (\vec{V} \cdot \vec{\nabla}) f = 0, \tag{3}$$

was solved along with the mass and momentum conservation equations. Surface tension was considered to be a component of the body force ($\vec{F}_b$) acting on the fluid free surface, by using the continuum surface force (CSF) model [15]. Fluid flow boundary conditions were no-slip and no-penetration at solid surfaces. Laplace's equation was used to determine the pressure jump across free liquid surfaces. Advancing and receding contact angles were specified along liquid–solid contact lines. Based on measurements from photographs [13], the dynamic advancing and receding contact angles for tin on stainless steel were set as 140° and 40°, respectively. The dynamic contact angle between liquid tin and solid tin was assumed to be 90°.

The conservation of energy equation was solved to calculate heat transfer in the droplet. In order to have only one dependent variable in the energy equation, i.e. enthalpy $h$, the enthalpy transforming model of Cao et al. [16] was employed. Neglecting viscous dissipation, the energy equation can be rewritten as [17]:

$$\rho \frac{\partial h}{\partial t} + \rho(\vec{V} \cdot \vec{\nabla}) h = \nabla^2(\beta h) + \nabla^2 \phi. \tag{4}$$

The main advantage of this method is that it allows simultaneous solution of the energy equation in both liquid and solid phases. Assuming that phase change occurs at a single temperature (as is the case in pure substances), the enthalpy coefficient ($\beta$) and source term ($\phi$) for the solid phase ($h \leqslant 0$) become $\beta = k_s/C_s$ and $\phi = 0$, where $k$ represents the thermal conductivity and $C$ the specific heat. At the liquid–solid interface, where both phases co-exist ($0 < h < H_f$) $\beta$ and $\phi$ are both

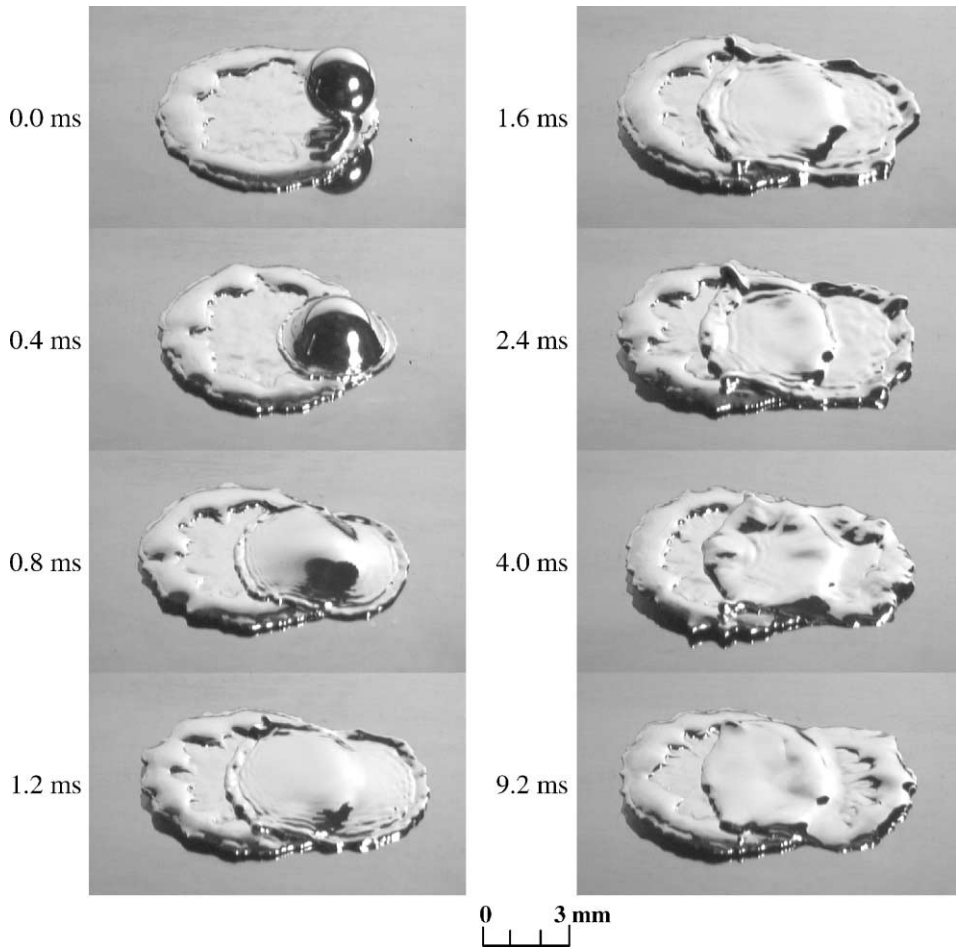


Fig. 3. Impact of a 2.2 mm diameter tin droplet landing with a velocity of 2.5 m/s on a splat formed by depositing another identical drop. The center of the second droplet is offset 2.0 mm from that of the first.

reduced to zero and in the liquid phase ($h \geqslant H_f$) they become $\beta = k_l/C_l$ and $\phi = -H_f k_l/C_l$. Densities were assumed to be constant and equal to each other in both phases. The enthalpy calculated from Eq. (3) can be converted to temperature by:

$$T = T_m + \frac{1}{k}(\beta h + \phi), \tag{5}$$

where $T_m$ is the melting point of the droplet.

The effect of convection and radiation from the free liquid surface was neglected. The heat flux ($q$) at the of droplet-substrate interface was:

$$q = \frac{(T - T_w)_{substrate}}{R_c}, \tag{6}$$

where $R_c$ represents the thermal contact resistance between droplet and substrate per unit area and $T_w$ the substrate temperature. A value of $R_c = 2 \times 10^{-6}$ m$^2$ K/W

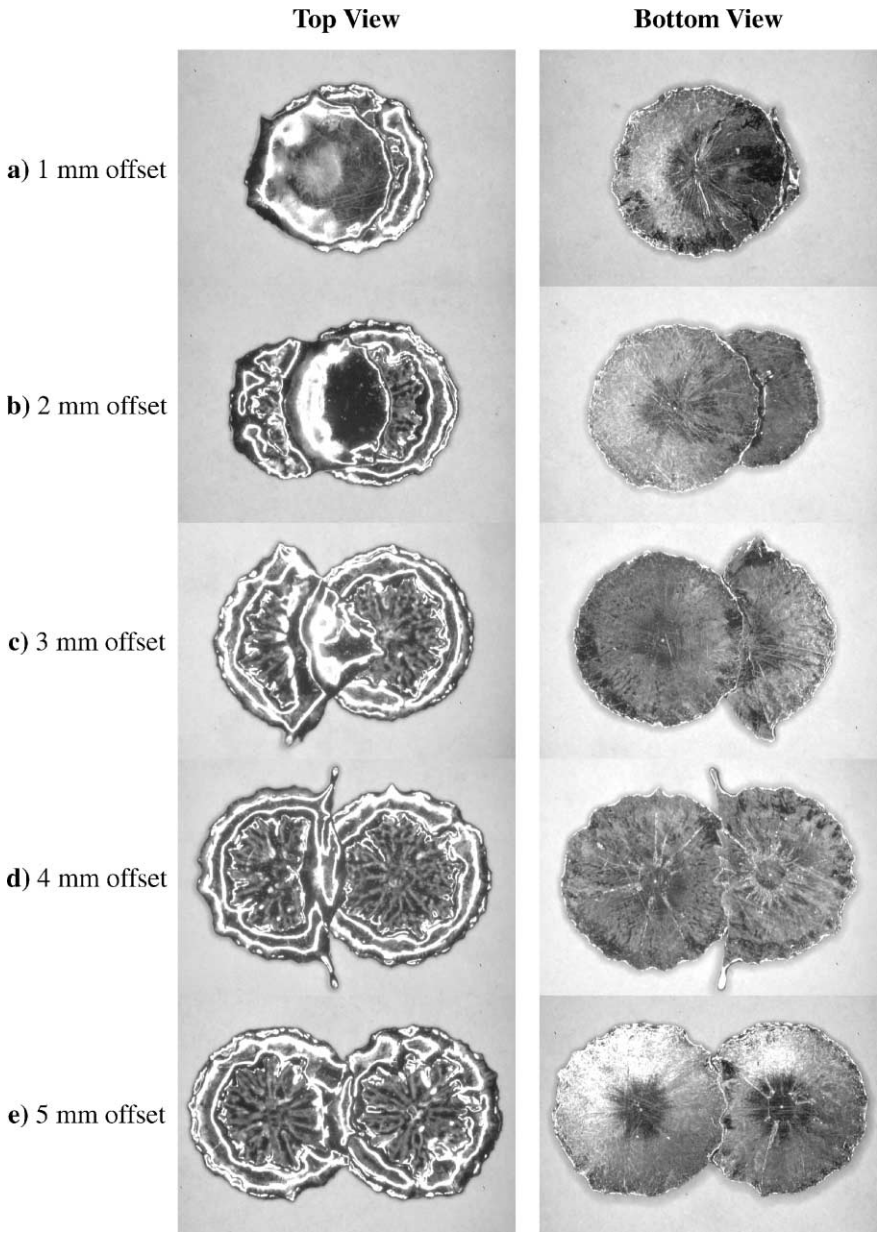


Fig. 4. Top and bottom views of splats, each formed by the deposition of 2.2 mm diameter tin droplets on top of another, with offset distances varying from 1.0 to 5.0 mm.

was used at all interfaces in the model, based on published data in the literature [13]. An adiabatic boundary condition was applied at the droplet free surface and on the exposed portions of the substrate that were not covered by the droplet. Heat transfer within the substrate was by conduction alone. Properties of tin and stainless steel were taken from Incropera et al. [18] and Boyer et al. [19]. Properties of molten droplets were assumed to be constant, but substrate thermal properties were allowed to vary with temperature (Table 1).

### 3.2. Phase change and solidification

Advance of the solidification front was described by a modified version of the fixed velocity method [15], employing a special case of two-phase flow, in which the first phase is the liquid, with volume fraction $\Theta$, and the second phase is the solid, with volume fraction $(1-\Theta)$. The volume fraction $\Theta$ is a parameter whose value is equal to one in the liquid and zero in the solid. The volume-of-fluid $(f)$ is the fraction of cell volume occupied by the fluid. When both phases exist in a cell, (i.e.,

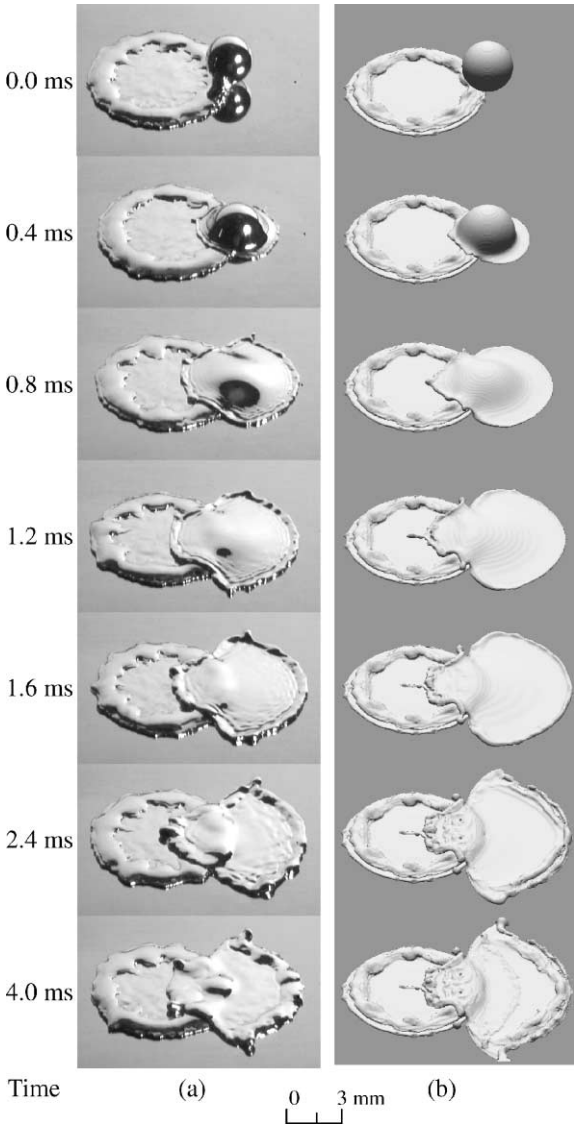


Fig. 5. Comparison of photographs and computer generated images of a 2.2 mm diameter tin droplet landing with a velocity of 2.5 m/s at a point 3.0 mm from the center of a solidified splat.

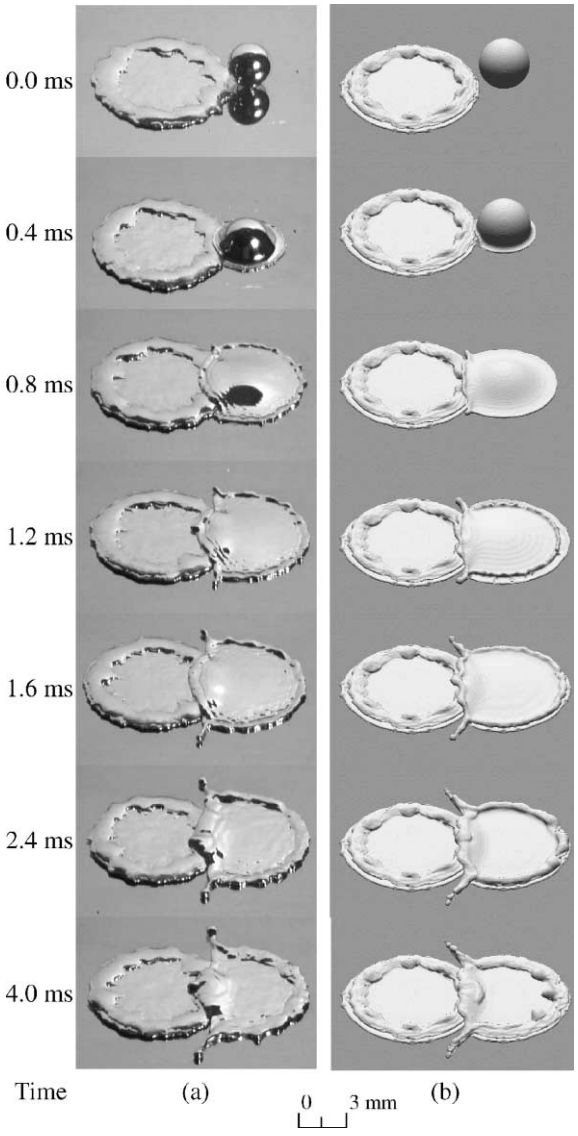


Fig. 6. Comparison of photographs and computer generated images of a 2.2 mm diameter tin droplet landing with a velocity of 2.5 m/s at a point 4.0 mm from the center of a solidified splat.

liquid flows over its own solid) $f$ is the fraction of a cell volume occupied by both liquid and solid while $\Theta$ is the liquid fraction of $f$ existing in the cell.

For cells with a value of $\Theta$ satisfying $0 < \Theta < 1$, both phases exist; the liquid portion $(\Theta)$ is free to flow while the remaining portion $(1-\Theta)$ is solid. Eqs. (1)–(3) for these cells are modified to [9]:

$$\vec{\nabla}\cdot(\Theta\vec{V}) = 0, \tag{7}$$

$$\frac{\partial(\Theta\vec{V})}{\partial t} + (\Theta\vec{V}\cdot\vec{\nabla})\vec{V} = \frac{-\Theta}{\rho}\vec{\nabla}p + \Theta\nu\nabla^2\vec{V} + \frac{\Theta}{\rho}\vec{F}_{\mathrm{b}}, \tag{8}$$

$$\frac{\partial f}{\partial t} + (\Theta\vec{V}\cdot\vec{\nabla})f = 0. \tag{9}$$

The method of solution of Eqs. (7)–(9) is a two-step projection method described in detail by Bussmann et al. [14]. Young's algorithm was applied to regenerate the free surface interface by locating a plane within each free surface cell. The computational algorithms used for Eqs. (7)–(9) were the same as those applied in cells with no solid, except that the solidified region was treated as a liquid with zero velocity.

A no-slip condition boundary condition was applied at the solidification front and contact angles prescribed at all liquid–solid contact lines. Since these lines were moving we first needed to locate their position in the model. At the solidification front the contact angle was defined as the angle between the unit normal vector, $\hat{n}_{\mathrm{l}} = \vec{\nabla}f/|\vec{\nabla}f|$, pointing into the liquid phase and the unit normal, $\hat{n}_{\mathrm{s}} = -\vec{\nabla}\Theta/|\vec{\nabla}\Theta|$, pointing into the solid phase at every point along the contact line. Normals were evaluated at any vertex of the solid cells adjacent to the contact line. The angle between the two unit normals

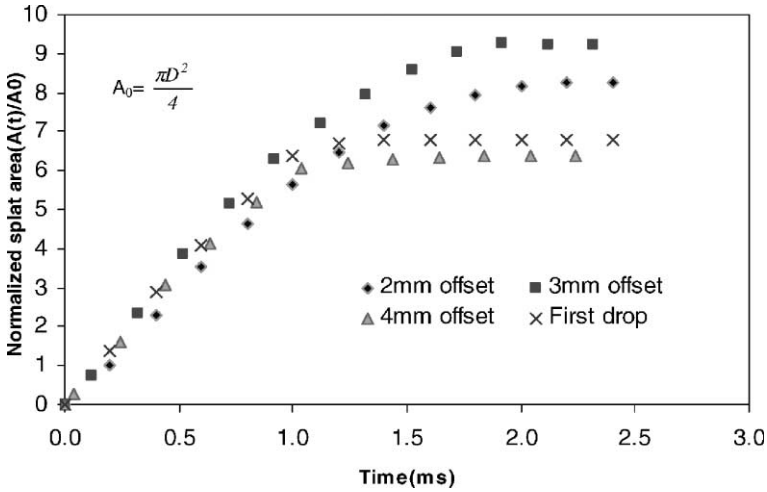


Fig. 7. Variation of droplet surface area during impact of a 2.2 mm diameter tin droplet on a solidified splat, with varying center offset distance.

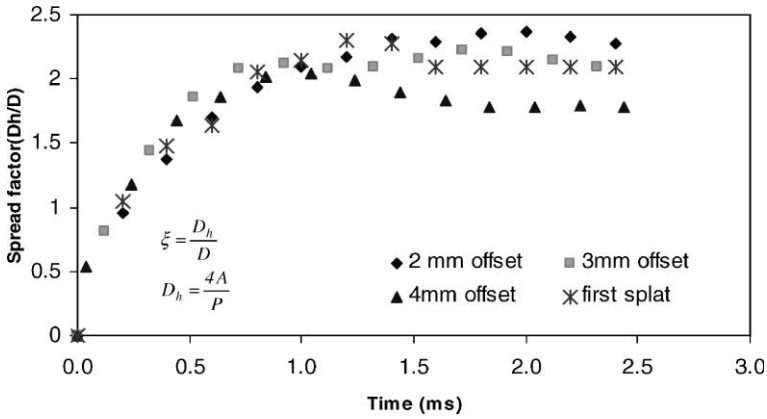


Fig. 8. Variation of spread factor during impact of a 2.2 mm diameter tin droplet on a solidified splat, with varying center offset distance.

was obtained from $\gamma = \cos^{-1}(\hat{n}_l \cdot \hat{n}_s)$. As solidification progressed, the direction of unit normals $\hat{n}_l$ and $\hat{n}_s$ changed with location on the contact line.

Simulations were carried out on a Sparc SUNW, Ultra-4, machine using a mesh that had uniform grid spacing in $x$, $y$ and $z$ directions, equal to 20 cells per radius of the impacting droplets. Symmetry about the plane passing through the droplet centers allowed us to confine our calculation domain to half of each droplet.

## 4. Results and discussion

Fig. 2 shows a sequence of photographs of the impact of a 2.2 mm tin droplet, landing with a velocity of 2.5 m/s on a splat formed by another identical droplet, with the center of the second drop offset by 1.0 mm from that of the first. The time of each picture, measured from the instant of impact of the second drop, is indicated below every frame. The droplet spread out radially into a disk-shape, almost entirely covering the lower splat. Cross-sections through the splats showed that they had bonded together well, with the interface between them having melted and resolidified sufficiently to join the two droplets.

Fig. 3 shows a similar set of pictures of droplet impact, under conditions almost identical to those of Fig. 2, the only difference being that the offset distance of the second droplet was increased to 2 mm. The spreading droplet was closer to the edge of the first splat and a

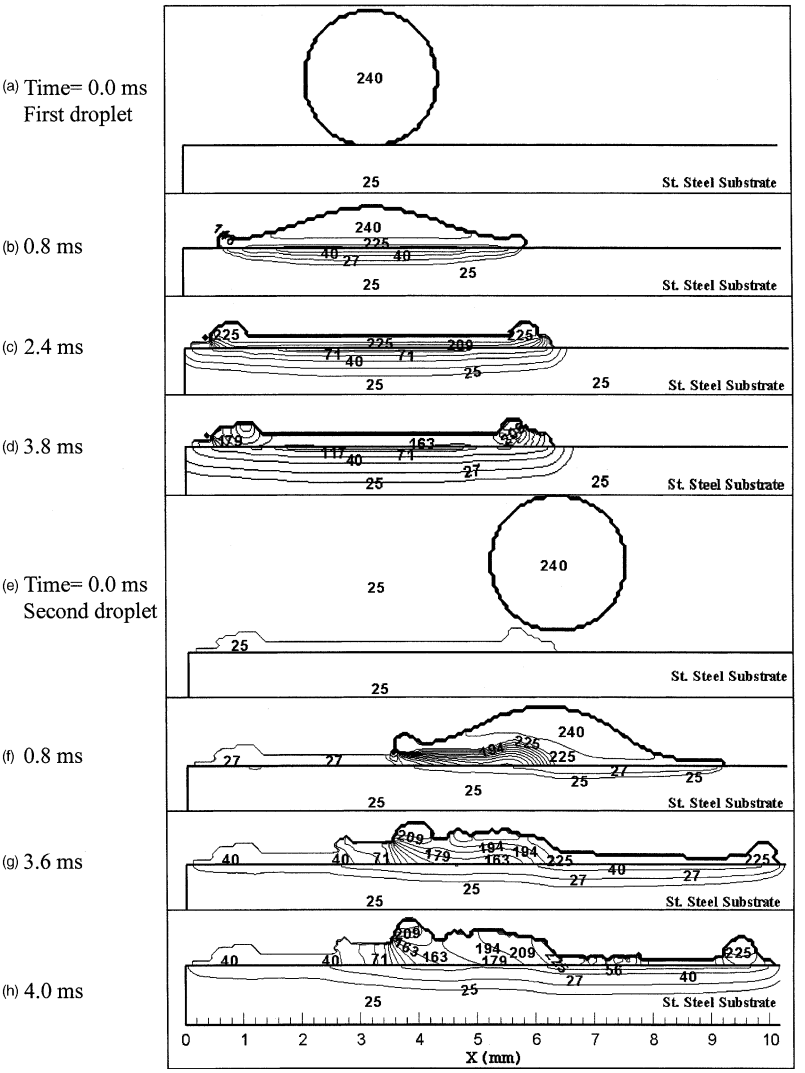


Fig. 9. Calculated temperature distributions inside 2.2 mm diameter tin droplets, initially at 240 °C, landing on a stainless steel surface at 25 °C. The second droplet lands with its center 3.0 mm from that of the first, after the first droplet and the substrate have cooled to 25 °C.

larger portion of it flowed onto the steel substrate. It therefore assumed a shape more elongated than that of the droplet with 1 mm offset.

The final shape of the second droplet was very sensitive to the location of its point of impact. Fig. 4 shows photographs of solidified splats, photographed from both top and bottom, collected from droplet impacts with offset spacing varying from $L = 1$ to 5 mm. Even small changes in impact position strongly affected the splat morphology. Droplets landing with $L = 1.0$ and 2.0 mm spread mostly on the surface of the first splat and solidified in a roughly circular shape (Fig. 4a and b). At an offset distance of 3.0 mm the second droplet landed almost exactly on the edge of the first splat. Most of the molten tin spread onto the steel substrate, and only a small portion climbed over the solid splat (Fig. 4c). When $L$ was increased to 4.0 mm, the droplet initially landed on the steel substrate. As it spread it hit the edge of the previous splat so that liquid was diverted to either side, producing two distinct fingers (Fig. 4d). A droplet landing 5.0 mm from the first did not touch it until almost the end of spreading, and the two were joined with each other only over a very small area (Fig. 4e).

The numerical model was quite successful in predicting the dynamics of droplet impact and the shapes of splats formed by droplet interaction. Fig. 5 shows both photographs and computer-generated images of a tin droplet landing on a solidified splat, with their centers spaced 3 mm apart. In the numerical simulations initial droplet temperature was set to 240 °C and impact velocity to 2.5 m/s. When the first droplet landed on the steel substrate molten metal jetted out, away from the center of the droplet. The rate of solidification was fastest around the rim of the spreading drop, where it first contacted the colder substrate, and the metal began to solidify there. Obstruction of flow by the solidified layer around the splat rim and surface tension pulling back the liquid made the molten layer recoil toward the center of splat until the droplet was completely frozen. As a result, the solidified splat was thicker around its periphery than at its center, which we also observed in experiments (see Fig. 5, $t = 0.0$ ms). In simulations the temperature of the splat and the substrate were reset to 25 °C once the first droplet had fully solidified, to account for cooling in the experiments, and then the second droplet was introduced. The impacting droplet landed on the edge of the splat (Fig. 5, $t = 0$ ms) and then spread, most of it flowing onto the steel substrate. A small portion of the molten tin climbed over the splat ($t = 2.4$ ms). The model captured the salient features of the flow well. Small discrepancies between the experiment and model, especially near the advancing liquid–solid contact line, were largely due to uncertainties in the values used for the contact angle and local thermal contact resistance.

Fig. 6 shows comparisons between photographs and computer model predictions for droplet shape during impact at an offset distance of 4 mm. In this case the droplet initially landed on the steel surface (Fig. 6, $t = 0$ ms). As it jetted outwards it encountered the edge of the solid splat that acted as an obstacle, diverting most of the liquid to either side in the form of two fingers (Fig. 6, $t = 1.6$ ms). Only a small portion of the droplet climbed over the solidified mass of tin (Fig. 6, $t = 4.0$ ms).

The size to which a droplet spreads depends on its distance from the center of the splat below it. Fig. 7 shows the variation of droplet surface area ($A$), measured from images generated by the model, during

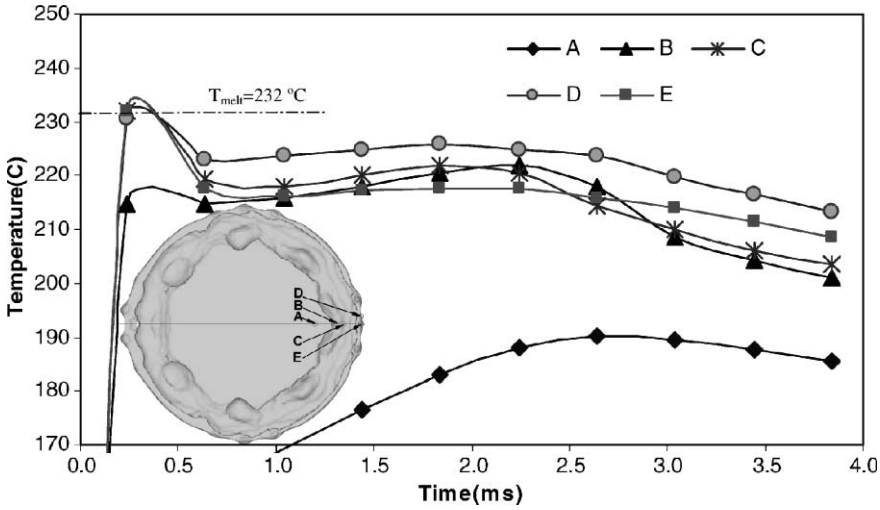


Fig. 10. Temperature variation with time at five points (labeled A–E) on the surface of the lower splat during the impact of a second drop 3.0 mm from the center of the first.

droplet impact. The area of a single droplet landing and solidifying on a steel surface increases by a factor of approximately 6.8. If a second droplet lands quite far (see Fig. 7, offset distance = 4 mm), there is relatively little interaction between the two drops and both drops spread about the same amount. If the second droplet is very close (offset distance = 2 mm), it flows off the edges of the first splat so that its surface area increases by a greater amount. But an intermediate offset distance (3 mm) leads to greatest spreading of the droplet (see Fig. 5) and produces the largest increase in surface area, almost 35% greater than that of a single drop.

Distortion of a droplet due to interactions with a splat on the surface increases both its surface area and perimeter ($P$). A useful length scale to describe spreading of the droplet during impact is the equivalent diameter $D_h = 4A/P$. Normalizing this by the initial droplet diameter we define the spread factor $\xi = D_h/d$. Fig. 8 shows the variation of $\xi$ during spreading of droplets with different values of $L$. All the droplets show approximately the same value of $\xi$, except for the case of $L = 4$ mm, in which case fingering led to a large perimeter length so that $\xi$ was smaller.

The numerical model was useful in calculating the temperature distribution in droplets during impact, as shown in Fig. 9. The first droplet of molten tin, at an initial uniform temperature of 240 °C, landed on the stainless steel substrate at 25 °C (Fig. 9a). Conduction to the cold substrate rapidly cooled the droplet, so that by $t = 2.4$ ms (Fig. 9c) the temperature everywhere in it was below the melting point of tin (232 °C), and it was entirely frozen. Since solidification started at the edges of the drop the final splat was thicker at its periphery than at its center. Once the splat and substrate had cooled down, which was accomplished in the model by resetting all temperatures to 25 °C, the second droplet was introduced at an offset distance $L = 3$ mm (Fig. 9e). As it spread it was in contact with both the stainless steel substrate and the tin splat formed by the first droplet. Since the thermal diffusivity of tin is almost 10 times that of stainless steel [18], the area in contact with the splat

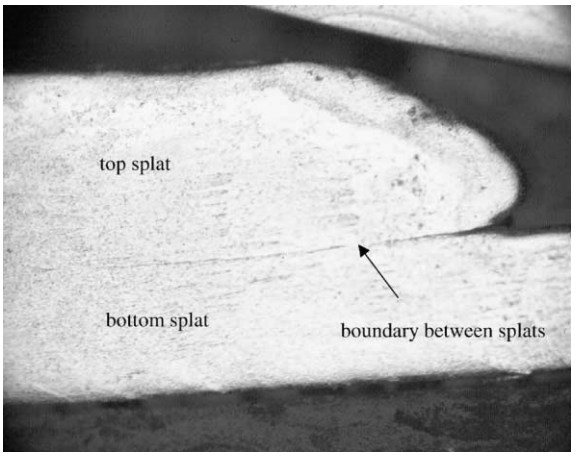


Fig. 11. Cross-section though splats formed by a 2.2 mm tin droplet deposited on top of another with their centers offset by 3.0 mm.

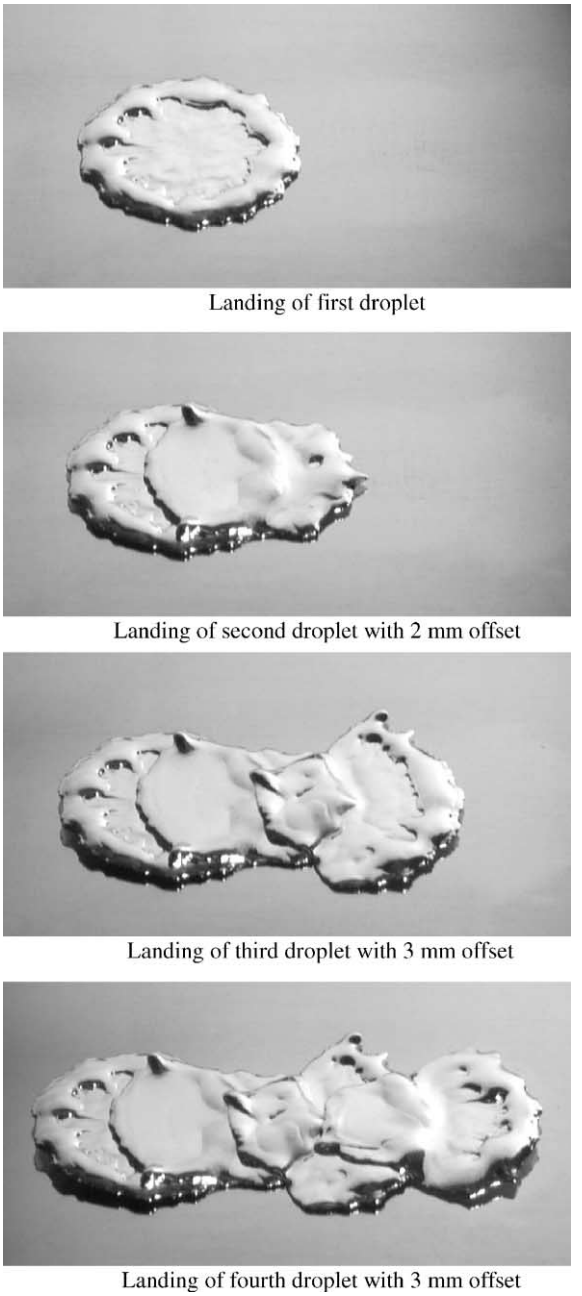


Fig. 12. Splats formed by depositing four tin drops along a straight line, with the center of each drop offset by 2.0, 3.0 and 3.0 mm respectively from that of the previous one.

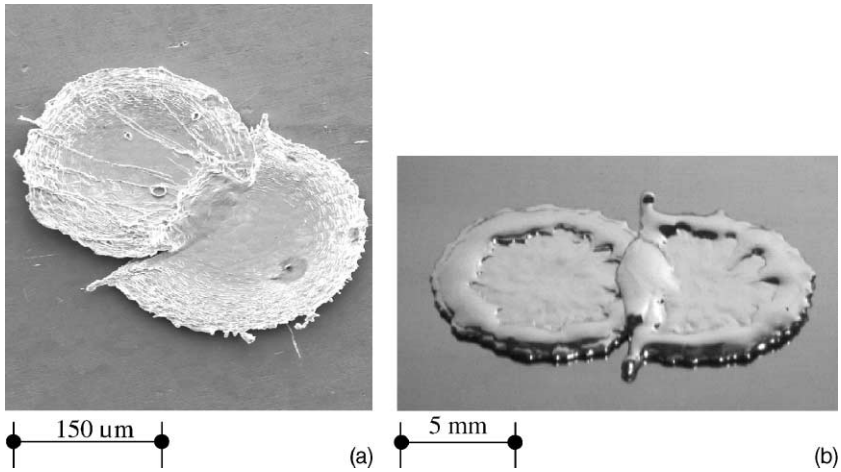


Fig. 13. (a) Nickel splats produced by melting 30–50 μm diameter particles in a plasma jet and propelling them at high velocity (70–90 m/s) onto a stainless steel substrate. (b) Tin splats formed by depositing a 2.2 mm diameter droplet with a velocity of 2.5 m/s on another splat, with their centers offset by 4.0 mm.

cooled faster (Fig. 9g and h). Heat conduction towards the colder portion of the droplet, which was in contact with the solid splat, raised the temperature at the interface between solid and molten tin, promoting remelting and bonding between the two droplets.

The temperature history of a particular point on the bottom splat, and remelting there, was sensitive to the local surface *topography*. Fig. 10 shows the temperature variation at five points (labeled A–E) on the surface of the bottom splat during impact of a second drop at an offset distance of 3.0 mm. Time $t = 0$ corresponds to the instant of deposition of the second drop. The temperature at points C, D and E (which were closest to the edge of the splat where the second droplet landed) briefly exceeded the melting point of tin, so that remelting occurred at those locations. We sometimes observed significant differences in temperature between two locations very close to each other, such as points D and E, depending on the surrounding surface shape and flow over it. As the second drop spread further, towards the center of the lower splat, the temperature of the solid under the advancing interface remained below the melting point (see Fig. 10, points A and B) and there was no bonding between the two splats. Examination of splats collected from experiments confirmed this observation. Fig. 11 is a micrograph of the cross-section through splats formed by a droplet being deposited on top of another, with their centers offset by 3 mm. Near the edge of the top splat the boundary between the two is clearly visible, whereas closer to its center the interface between them disappears, showing evidence of remelting and fusing of the splats.

We focused only on two-droplet interactions in this study. In our model of thermal spray coating [10] we had assumed that the shape assumed by an impinging drop was determined only by the distance of its center from that of the nearest splat under it. Experimental evidence offered some support for this conjecture. Fig. 12 shows a sequence of photographs taken during the deposition of four droplets along a straight line. The distances between the centers of successive drops were 2, 3 and 3 mm respectively. The shape of the splats appeared similar to those formed by two-droplet interactions (see Fig. 4) with the same center spacing, and did not appear greatly influenced by the presence of other drops.

All the experiments described in the paper were done with relatively large (2.2 mm) and slow (2.5 m/s) droplets, whereas those in most applications are much smaller and travel with considerably greater speeds. However, even under such conditions the shapes of splats formed by droplet interaction appear to be very similar to those that we observed. Fig. 13a shows nickel splats produced by melting 40–70 μm diameter particles in a plasma jet and propelling them at high velocity (50–70 m/s) onto a stainless steel substrate. Their shape closely resembles that of tin splats photographed in our experiments (Fig. 13b). Simulations of impinging nickel droplets, and their interactions, have shown the fluid mechanics and heat transfer that occur during droplet impact and solidification to be qualitatively quite similar to those observed in the present study [20].

## 5. Conclusions

The final shape of a 2.2 mm molten tin droplet landing on a splat formed by the spreading of another identical drop was a function of the spacing between their centers. Droplets landing at small offset distances (1.0–2.0 mm) landed on the surface of the first splat,

spread and solidified in a roughly circular shape. At a larger spacing (4.0–5.0 mm) the second droplet initially landed on the steel substrate and hit the edge of the first drop as it spread, producing a non-circular splat. During droplet spreading the variation of the equivalent diameter $D_h = 4A/P$ with time was approximately the same for all drops, even those that had quite irregular shapes.

A three-dimensional model of droplet impact and solidification was able to predict splat shapes, and their variation with distance between droplet centers, quite accurately. By following the temperature variation at different points on the surface of the first splat we could identify locations where remelting occurred so that the splats fused together.

The splat shapes observed in experiments with large tin droplets qualitatively resembled those obtained by plasma spraying nickel powders on a steel surface. Shapes assumed by spreading drops appear to be most influenced by their distance from the center of the nearest splat under them.

## Acknowledgements

This research was supported by the Natural Sciences and Engineering Research Council of Canada, Materials and Manufacturing Ontario and members companies of the Centre for Advanced Coating Technologies at the University of Toronto.

## References

[1] G. Trapaga, J. Szekely, Mathematical modeling of the isothermal impingement of liquid droplets in spraying processes, Metall. Trans. B 22 (1991) 901–914.

[2] H. Liu, E.J. Lavernia, R. Rangel, Numerical simulation of substrate impact and freezing of droplets in plasma spray processes, J. Phys. D: Appl. Phys. 26 (1993) 1900–1908.

[3] Z. Zhao, D. Poulikakos, J. Fukai, Heat transfer and fluid dynamics during the collision of a liquid droplet on a substrate-I. Modeling, Int. J. Heat Mass Transfer 39 (13) (1996) 2771–2789.

[4] M. Bertagnolli, M. Marchese, G. Jacucci, I.St. Doltsinis, S. Noelting, Thermomechanical simulation of the splashing of ceramic droplets on a rigid substrate, J. Comput. Phys. 133 (1997) 205–221.

[5] M. Pasandideh-Fard, R. Bhola, S. Chandra, J. Mostaghimi, Deposition of tin droplets on a steel plate: simulations and experiment, Int. J. Heat Mass Transfer 41 (19) (1998) 2929–2945.

[6] J.M. Waldvogel, D. Poulikakos, Solidification phenomena in picoleter size solder droplet deposition on a composite substrate, Int. J. Heat Mass Transfer 40 (1997) 295–309.

[7] D. Attinger, Z. Zhao, D. Poulikakos, An experimental study of molten microdroplet surface deposition and solidification: Transient behavior and wetting angle dynamics, J. Heat Transfer 122 (3) (2000) 544–556.

[8] L.L. Zheng, H. Zhang, An adaptive level set method for moving-boundary problems: application to droplet spreading and solidification, Numer. Heat Transfer, Part B 37 (2000) 437–454.

[9] M. Pasandideh-Fard, J. Mostaghimi, S. Chandra, On a three dimensional model of free surface flows with heat transfer and solidification, in: Proceeding of the 3rd ASME/JSME Joint Fluids Engineering Conference, San Francisco, California, 1999, FEDSM99-7112.

[10] R. Ghafouri-Azar, J. Mostaghimi, S. Chandra, M. Charmchi, A stochastic model to simulate formation of a thermal spray coating, J. Thermal Spray Technol., in press.

[11] B. Kang, Z. Zhao, D. Poulikakos, Solidification of liquid metal droplets impacting sequentially on a solid surface, J. Heat Transfer 116 (1994) 436–445.

[12] B. Kang, J. Waldvogel, D. Poulikakos, Remelting phenomena in the process of splat solidification, J. Mater. Sci. 30 (1995) 4912–4925.

[13] S. Aziz, S. Chandra, Impact, recoil and splashing of molten metal droplets, Int. J. Heat Mass Transfer 43 (16) (2000) 2841–2857.

[14] M. Bussmann, J. Mostaghimi, S. Chandra, On a three-dimensional volume tracking model of droplet impact, Phys. Fluids 11 (6) (1999) 1406–1417.

[15] S. Shakeri, Effect of substrate properties on molten metal droplet impact, M.A.Sc. Thesis, University of Toronto, Toronto, Canada, 2001.

[16] Y. Cao, A. Faghri, W.S. Chang, A numerical analysis of Stefan problems for generalized multi-dimensional phase-change structures using the enthalpy transforming model, Int. J. Heat Mass Transfer 32 (1989) 1289–1298.

[17] M. Pasandideh-Fard, Droplet Impact and Solidification in a Thermal Spray Process, Ph.D. Thesis, University of Toronto, Toronto, Canada, 1998.

[18] F.P. Incropera, D.P. DeWitt, Fundamentals of Heat and Mass Transfer, 3rd ed., John Wiley and Sons, New York, 1990.

[19] H.E. Boyer, T.L. Gall, Metals Handbook, Desk Edition, American Society for Metals, Metals Park, Ohio, 1995.

[20] M. Pasandideh-Fard, J. Mostaghimi, S. Chandra, Modelling sequential impact of two molten droplets on a solid surface, in: Proceeding of 12th Annual Conference on Liquid Atomization and Spray Systems, Indianapolis, Indiana, May 16–19, 1999, pp. 265–269.